



Defining the optimal criterion for separating gases using polymeric membranes

Journal:	<i>Soft Matter</i>
Manuscript ID	SM-ART-10-2018-002012.R1
Article Type:	Paper
Date Submitted by the Author:	05-Nov-2018
Complete List of Authors:	Zhang, Kai; Columbia University, Chemical Engineering Kumar, Sanat; Columbia University,

Defining the optimal criterion for separating gases using polymeric membranes

Kai Zhang and Sanat K. Kumar*

Department of Chemical Engineering, Columbia University, New York, New York, 10027, USA

E-mail: sk2794@columbia.edu

Abstract

Polymeric membranes are efficient at separating gas mixtures, typically by exploiting a sieving mechanism. What controls the sieve size of a given polymer matrix is unclear, although one line of thought implies that the local cage size, defined by the dynamic motions of the glassy polymer matrix, is the relevant metric. Here, we use coarse-grained molecular dynamics simulations and show that the sieve size is defined by a static cavity size controlled by polymer chain stiffness (a packing-driven metric) combined with the local cage-like motions of the polymer host. The best separation performance for a pair of gases is when this combined metric is roughly half way between the diameters of the gases in question, with the static and dynamic quantities contributing roughly equally. For the various models simulated we find the existence of an upper bound correlation which passes through this optimal point and has a slope expected from the Freeman model, namely $\lambda = \left(\frac{d_B^2}{d_A^2} - 1\right)$, where the d 's correspond to the kinetic diameters of the gases in question. Our results thus demonstrate that the relevant free volume size that affect gas transport in these condensed phases is defined by both static and dynamic measures.

*To whom correspondence should be addressed

1 Introduction

Membrane based gas separations, which strive to maximize the permeability of a desired species (“flux”) while being selective towards it (“purity”), is the key to many clean energy applications, such as carbon dioxide capture and natural gas purification.¹ However, typical membranes exhibit a trade-off between permeability P_A and (ideal) selectivity $\alpha_{AB} = P_A/P_B$.^{2,3} The central goal for membrane design is thus to identify materials with both high P_A and α_{AB} . In the canonical solution-diffusion model, the permeability $P = D \times S$ is the product of the diffusivity (diffusion coefficient) D and solubility S .⁴ Although many types of materials, such as carbon, ceramics and zeolites, can be used to make membranes, 95% of the total industrial market consists of polymeric membranes.⁵ An early analysis of existing polymeric membranes suggested that $\log \alpha_{AB}$ is indeed negatively correlated with $\log P_A$ on a “Robeson plot” and this scatter plot is bounded from above by an empirical line $\log \alpha_{AB} = -\lambda \log P_A + \kappa$.⁶ Such an upper bound defines the optimal separation performance practically; understanding whether an upper bound limit exists theoretically and what factors affect its position is currently unknown.

Kinetic arguments proposed by Freeman shed some light on the quantitative form of the upper bound, for instance, that its slope depends purely on the sizes (d_A, d_B) of the two gases, $\lambda = (d_B/d_A)^2 - 1 \equiv \lambda_F$.⁷ In practice, it has been found that the position of the upper bound (i.e., its intercept) increases over time as more polymer materials are discovered, but that the slope itself remains relatively unchanged.⁸ The Freeman model is based on the assumptions that penetrant motion through polymers is an activated “anomalous” process⁹ with $D \sim e^{-E_a/k_B T}$ and the activation energy $E_a \sim d^2$. Previous computer simulations confirmed this picture under certain conditions and showed that the Robeson plot of a given polymer at different densities falls on a single line of slope λ_F .¹⁰ To move beyond this upper bound, new types of polymers with increasing local stiffness have been synthesized - these “thermally rearranged” polymers, for example, have performance that is better than the accepted upper bound correlation for commonly encountered polymers. Given these facts we ask if there is truly a well-defined upper bound correlation in a Robeson plot for a pair of gases. If so, what defines the intercept of this upper bound - this of

course assumes that the slope of the plot remains unchanged and equal to its Robeson value.

To answer this question, we perform coarse-grained molecular dynamics simulations of penetrant diffusion inside different types of polymers. To focus on the role of chain stiffness, we do not consider other effects such as solubility and non-spherical penetrants. We find that the chain stiffness alone provides a mechanism for the upper bound limit. The optimal chain stiffness (with best separation performance) can be identified by combining the concepts of *static* free volume and *dynamic* segmental motion, and we find that the optimal material (i.e., the one with the highest selectivity) corresponds to one where the combined "free volume" size is midway between the kinetic diameters of the gases in question.

2 Models and Methods

We disperse trace amounts ($N_s = 100$) of spherical penetrants into $N_c = 500$ coarse-grained polymers each of chain length $N_p = 120$ with monomer size σ . All monomers and penetrants are of the same mass, m_0 . Any pair (i, j) of particles (penetrants or monomers) interact via the purely repulsive Lennard-Jones (LJ) potential, $u_{LJ}(r_{ij}) = 4\epsilon[(\sigma_{ij}/r_{ij})^{12} - (\sigma_{ij}/r_{ij})^6] + \epsilon$ ($r_{ij} < r_c$), truncated and shifted at a cutoff $r_c = 1.12\sigma_{ij}$. Neighboring monomers on a chain are connected by finite extensible nonlinear elastic (FENE) bonds $u_{\text{FENE}}(r) = -0.5K_0R_0^2\ln[1 - (r/R_0)^2]$ ($r < R_0$) with force constant $K_0 = 30\epsilon/\sigma^2$ and $R_0 = 1.5\sigma$. Interactions within polymer chains also include a harmonic bond angle potential $u_{\text{angle}}(\theta) = K_1(\theta - \theta_1)^2$ with stiffness constant K_1 (in units of ϵ/rad^2) and equilibrium angle $\theta_1 = 109.5^\circ$ or 120° , as well as a dihedral angle potential $u_{\text{torsion}}(\phi) = K_2[1 + \cos(n\phi)]$ with stiffness constant K_2 (in units of ϵ) and the number of minima in one full rotation $n = 1$ or 3 . We tune these parameters in various regimes to implement five different polymer models, as summarized in Table 1. We focus on the penetrant pair with a fixed diameter ratio 0.8: $(d_A, d_B) = (0.32, 0.4)$ (in unit of σ), which falls in the range of typical gas size ratios in this coarse-grained description.¹¹ These sizes are motivated by the knowledge that one polymer segment represents a Kuhn length, with size $\sim 1\text{nm}$. Typical gas molecules of our

Table 1: Five polymer models used in this work and their number density range at fixed pressure $p = 12$ and temperature $T = 1$.

model	K_1	θ_1	K_2	n	ρ
I. angle-109.5	0–1000	109.5	0	–	1.026–1.000
II. torsion-300	300	109.5	1–100	3	0.990–0.755
III. trans	300	109.5	1–100	1	1.01–0.83
IV. angle-120	10–500	120	0	–	1.030–1.014
V. torsion-10	10	109.5	1–20	3	1.02–0.96

interest are 0.25–0.4 nm in size, justifying these choices. Note that we run the polymer with a given penetrant (either 0.32 or 0.4) so that we are only enumerating the diffusion of pure tracers in each case.

Molecular dynamics (MD) simulations are performed with a time step $\Delta t = 0.002$ (in units of $\tau_0 \equiv \sigma \sqrt{m_0/\varepsilon}$) at constant temperature $T = 1.0$ (in units of ε/k_B) and pressure $p = 12$ (in units of ε/σ^3), maintained by the Nose-Hoover thermostat and barostat using the LAMMPS package.¹² The corresponding monomer number density ρ in most systems is close to 1.0, except for extremely stiff chains (Table Table 1). After equilibrating the system for up to $t \sim 10^6$, over which no volume drift is noticeable on logarithmic time scale, we compute the mean squared displacement (MSD) Δr^2 of the penetrants and chain segments over a time period of $t \sim 10^5$. This time scale is long enough for the motion of small penetrants to become diffusive, yet still too short for any long-time chain relaxation to occur. Besides dynamic properties, we also measure the spatial distribution of static free volumes by randomly inserting probing hard spheres and growing them until they touch a neighboring particle.^{13,14} A final histogram is drawn over the diameters d_f of all successfully inserted spheres.

3 Results

We calculate the diffusion coefficients (D_A, D_B) of the penetrant pair with sizes $(d_A, d_B) = (0.32, 0.4)$ from their MSD in all the polymer systems. The corresponding diffusivity Robeson plot of $\log \alpha_{AB}^D$ vs. $\log D_A$ at $T = 1$ and $p = 12$ is constructed in Figure 1. The data point corresponding to

a flexible bead-spring polymer melt, with both bond angle and torsion interactions turned off, is marked by a cross. If the system were to obey the Freeman theory, the upper bound should follow the dashed line with a slope $\lambda_F = 0.5625$; we have previously showed that these trends can be realized by changing the density (pressure) of the flexible polymer systems, without changing chain architecture or interactions.¹⁰ By increasing the chain stiffness (either K_1 or K_2), the separation performance is able to move above the flexible chain upper bound. The actual trends can be divided into two categories. As chain stiffness increases through the addition of a bond angle potential (cases I and IV), the system goes from right to left on the Robeson plot (D_A decreases) when bond angle is not rigid ($K_1 \lesssim 300$). At the same time the data “exceed” the flexible chain upper bound. The addition of a torsional angle potential causes the curve to move from right to left when bond angle is close to be fixed ($K_1 \gtrsim 300$). The best separation performance is achieved on the upper left corner in Figure 1, where the large K_1 makes the bond angle θ almost fixed at θ_1 . After reaching this optimal spot, increases in stiffness (K_2) will not lead to any further upward movement on the Robeson plot. It appears that there is a well-defined upper bound for this collection of models - we believe that this corresponds to a line with slope λ_F passing through the green point on the upper left hand region of the figure.

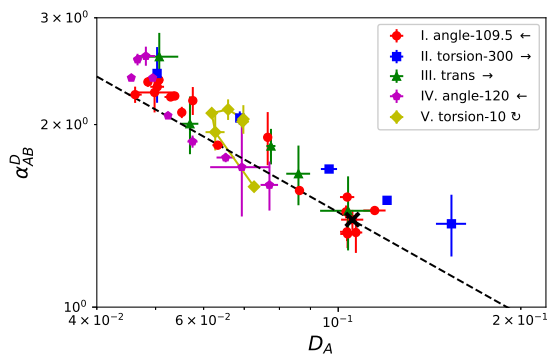


Figure 1: The diffusivity Robeson plot for the five polymer models at $T = 1$ and $p = 12$. The arrows in the legend point to the direction of increasing chain stiffness (the trend for model V is non-monotonical). The result for totally flexible chains ($K_1, K_2 = 0$) is marked by a black cross, through which an upper bound assuming the Freeman theory slope $\lambda_F = 0.5625$ is drawn (dashed line). Error bars are estimated from two independent simulations.

To understand these trends, we quantify the size of *static* free volumes in the polymers. For

each polymer system, we take four equilibrated configurations and insert 10000 probing spheres in the background of frozen polymers. The spheres are grown till they contact one of the chain monomers. These probing spheres are randomly distributed in space (Figure 2 inset). The histograms of the resulting maximum sphere diameters d_f are collected and fitted with the distribution $p(d_f) = \sqrt{2/\pi} \langle d_f \rangle^{-2} e^{-d_f^2/2\langle d_f \rangle^2}$ ($d_f \geq 0$), which is characterized by one parameter – the average diameter $\langle d_f \rangle$. As chain stiffness, as characterized by the torsional potential, increases, the system exhibits larger voids (Figure 2). However, the stiffness of the bond angle potential (K_1 alone) only has a minor effect on $p(d_f)$. This last result is a manifestation of the fact that, although we increase bond stiffness by increasing K_1 , the chain has considerable rotational flexibility. Thus, the chains pack well and there is basically no change to the static free volume size. The addition of the torsional angle potential with say a single dominant minimum, on the other hand, tends to force the chains to be planar - poor packing of these planar objects then leads to additional free volume. This trend, of course, cannot go on without bound since a transition to a liquid-crystalline (or a crystal) will take place.

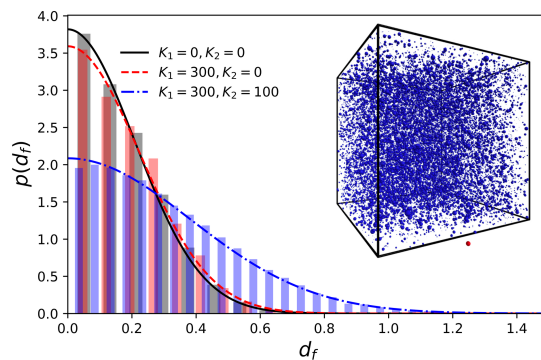


Figure 2: The distribution $p(d_f)$ of the diameters d_f of probing spheres fitted by the half-normal distribution for three polymer systems. Inset: an example snapshot of the spatial distribution of probing spheres (blue), compared to the size of one monomer outside of the simulation box (red).

We next turn to a dynamic measurement of void sizes based on the Debye-Waller (DW) factor¹⁵ of chain MSD at a certain time τ , $u(\tau) = \sqrt{\Delta r^2(\tau)}$. Previous studies have suggested that the DW factor is an appropriate measure of the local elastic fluctuations of the polymer matrix, which facilitate the activated motion of large enough penetrants even when the polymer is in its deeply

quenched glassy state.¹⁶ We pick $\tau = 100$, a typical intermediate timescale that separates the short-time and long-time segmental motions (Figure 3) and find that the resulting u exhibits a sigmoidal dependence on chain stiffness (Figure 3 inset).

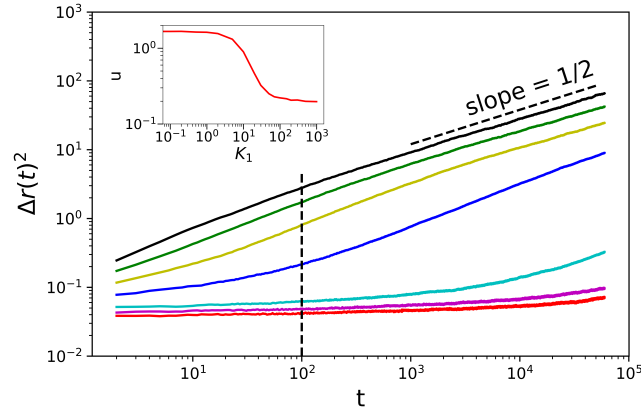


Figure 3: The segmental MSD for polymer model I at $K_1 = 0, 5, 10, 20, 50, 100, 300$ (from top to bottom), whose height at $\tau = 100$ (vertical dashed line) is used to measure chain dynamics. Inset: the corresponding DW factor $u(\tau = 100)$ as a function of K_1 .

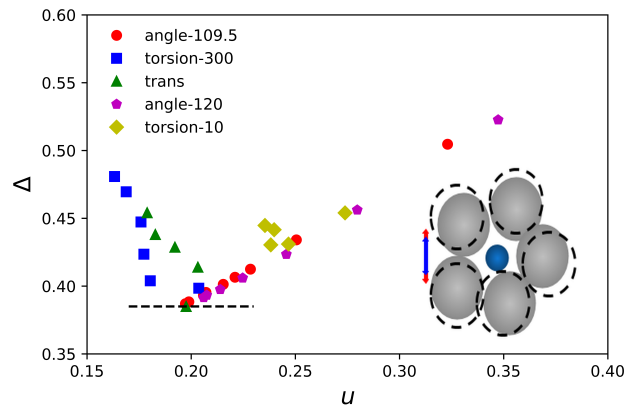


Figure 4: The effective cage size is $\Delta = \langle d_f \rangle + u$ versus DW factor u for the five polymer models. Optimal separation occurs when Δ is minimized (dashed line). Inset: a penetrant is trapped inside the cage formed by segments, which defines a static free volume size d_f (blue arrow). The slow motion of segments adds a dynamic contribution (red arrow) to the overall cage size.

Small penetrants like gases diffuse through a polymer matrix via an activated hopping mechanism, when the segmental dynamics becomes caged and the penetrant size is larger than a critical value defined by the surrounding cage size.¹⁰ Here, we propose a quantity $\Delta = \langle d_f \rangle + u$, which

characterizes the effective cage size felt by the penetrant, by combining the contributions from both static free volume resulting from polymer packing and dynamic fluctuations due to chain movement (Figure 4 inset). When Δ is plotted against u for all the polymer systems we studied, a minimum Δ_{\min} appears at $u \approx 0.2$ ($\Delta=0.37$), which corresponds to the optimal separation spot in the Robeson plot (Figure 1 and Figure 4). Interestingly, this optimal effective cage size is between the sizes of the two gases, i.e. $d_A < \Delta_{\min} < d_B$, which may explain why the smaller gas is most efficiently separated from the larger one by polymers with $\Delta = \Delta_{\min}$. As mentioned above, u is a measure for chain stiffness (or T_g), and thus divides polymers into two extreme categories in Figure 4. At large u (small d_f), polymers are dense but flexible rubbers or melts. At small u (large d_f), polymers are sparse but rigid glasses. Polymers with best separation performance are stiff enough to form stable cages, but not too stiff to open up big cavities due to thermal motions of the chain segments. We thus conclude that both static and dynamic metrics appear to be in balance in this sweet spot corresponding to the most selective polymer gas separation medium, which also appears to have the the largest intercept for an upper bound correlation in a Robeson plot.

4 Conclusion

In this work, we show that chain stiffness can impose a theoretical limit for the upper bound of the Robeson plot of a polymeric membrane's gas separation performance. This limit can be quantitatively approached by considering the static free volume and the dynamic segmental motion together. Our findings can help to explain why the separation performance of semi-rigid polymers, e.g. polymers with intrinsic microporosity (PIMs) and thermally rearranged polymers (TRs), can exceed ordinary polymers.¹⁷ Early on, it was recognized that, to improve separation performance, one should inhibit intersegmental packing (increase d_f) while simultaneously hindering the backbone mobility (reduce u).¹⁸ Such a protocol corresponds to reducing u on the right branch of our Δ - u plot (above $u \gtrsim 0.2$). Here we show that this process has an apparent optimum at the limit of best separation, beyond which the trend reverses. Finally, it is worth noting that the real upper bound

in experimental systems depends on other factors not considered here. For instance, although solubility is often secondary to diffusivity,¹⁰ certain systems are actually solubility-selective.¹⁹ Also, many real gases are not spherically shaped; in these cases entropic factors can also contribute significantly to the overall separation.²⁰

Conflicts of interest

There are no conflicts to declare.

Acknowledgments

We acknowledge primary financial support from the National Science Foundation under grant DMR-1507030.

References

1. Galizia, M.; Chi, W. S.; Smith, Z. P.; Merkel, T. C.; Baker, R. W.; Freeman, B. D. 50th anniversary perspective: Polymers and mixed matrix membranes for gas and vapor separation: A review and prospective opportunities. *Macromolecules* **2017**, *50*, 7809–7843.
2. Ghosal, K.; Freeman, B. D. Gas separation using polymer membranes: an overview. *Polymers for Advanced Technologies* **1994**, *5*, 673–697.
3. Park, H. B.; Kamcev, J.; Robeson, L. M.; Elimelech, M.; Freeman, B. D. Maximizing the right stuff: The trade-off between membrane permeability and selectivity. *Science* **2017**, *356*, 1137.
4. Wijmans, J. G.; Baker, R. W. The solution-diffusion model: a review. *Journal of Membrane Science* **1995**, *107*, 1–21.
5. Hennessy, J.; Livingston, A.; Baker, R. Membranes from academia to industry. *Nature Materials* **2017**, *16*, 280–282.

6. Robeson, L. M. Correlation of separation factor versus permeability for polymeric membranes. *Journal of Membrane Science* **1991**, *62*, 165–185.
7. Freeman, B. D. Basis of permeability/selectivity tradeoff relations in polymeric gas separation membranes. *Macromolecules* **1999**, *32*, 375–380.
8. Robeson, L. M. The upper bound revisited. *Journal of Membrane Science* **2008**, *320*, 390–400.
9. Müller-Plathe, F. Diffusion of penetrants in amorphous polymers: A molecular dynamics study. *The Journal of Chemical Physics* **1991**, *94*, 3192–3199.
10. Zhang, K.; Meng, D.; Müller-Plathe, F.; Kumar, S. K. Coarse-grained molecular dynamics simulation of activated penetrant transport in glassy polymers. *Soft Matter* **2018**, *14*, 440–447.
11. Zhang, R.; Schweizer, K. S. Statistical Mechanical Theory of Penetrant Diffusion in Polymer Melts and Glasses. *Macromolecules* **2016**, *49*, 5727–5739.
12. Plimpton, S. Fast parallel algorithms for short-range molecular dynamics. *Journal of Computational Physics* **1995**, *117*, 1–19.
13. Nagel, C.; Schmidtke, E.; Günther-Schade, K.; Hofmann, D.; Fritsch, D.; Strunskus, T.; Faupel, F. Free volume distributions in glassy polymer membranes: comparison between molecular modeling and experiments. *Macromolecules* **2000**, *33*, 2242–2248.
14. Kruse, J.; Kanzow, J.; Rätzke, K.; Faupel, F.; Heuchel, M.; Frahn, J.; Hofmann, D. Free volume in polyimides: positron annihilation experiments and molecular modeling. *Macromolecules* **2005**, *38*, 9638–9643.
15. Larini, L.; Ottochian, A.; De Michele, C.; Leporini, D. Universal scaling between structural relaxation and vibrational dynamics in glass-forming liquids and polymers. *Nature Physics* **2008**, *4*, 42.
16. Meng, D.; Zhang, K.; Kumar, S. K. Size-dependent penetrant diffusion in polymer glasses. *Soft Matter* **2018**, *14*, 4226–4230.

17. Koros, W. J.; Zhang, C. Materials for next-generation molecularly selective synthetic membranes. *Nature Materials* **2017**, *16*, 289.
18. Koros, W.; Coleman, M.; Walker, D. Controlled permeability polymer membranes. *Annual Review of Materials Science* **1992**, *22*, 47–89.
19. Freeman, B.; Pinnau, I. Separation of gases using solubility-selective polymers. *Trends in Polymer Science* **1997**, *5*, 167–173.
20. Singh, A.; Koros, W. Significance of entropic selectivity for advanced gas separation membranes. *Industrial & Engineering Chemistry Research* **1996**, *35*, 1231–1234.